PERGAMON

International Journal of Heat and Mass Transfer 45 (2002) 3919–3932

International Journal of HEAT and MASS TRANSFER

www.elsevier.com/locate/ijhmt

Pool boiling heat transfer on small heaters: effect of gravity and subcooling

Jungho Kim [a,*], John F. Benton [b], Derek Wisniewski [a]

[a] Department of Mechanical Engineering, University of Maryland, 2181 Glenn L Martin Hill, College Park, MD 20742, USA
[b] Schlumberger Completions Product Center, 7030 Ardmore Street, Houston, TX 77054, USA

Received 19 November 2001; received in revised form 7 March 2002

Abstract

Measurements of space and time resolved subcooled pool boiling of FC-72 in low, earth, and high gravity environments were made using a microscale heater array. Data from each heater in the array were synchronized with high-speed digital video. The boiling behavior was dominated by the formation of a large primary bubble on the surface which acted as a "sink" for many smaller bubbles surrounding it. Dryout of the heater occurred under the primary bubble. For a given superheat, this primary bubble was observed to increase in size with bulk fluid temperature. Boiling curves at various subcoolings and gravity levels are presented. © 2002 Published by Elsevier Science Ltd.

1. Introduction

Boiling is a complex phenomenon where hydrodynamics, heat transfer, mass transfer, and interfacial phenomena are tightly interwoven. An understanding of boiling and critical heat flux in microgravity environments is of importance to space-based hardware and processes such as heat exchange, cryogenic fuel storage and transportation, electronic cooling, and material processing due to the large amounts of heat that can be removed with relatively little increase in temperature. Although research in this area has been performed in the past four decades, the mechanisms by which heat is removed from surfaces in microgravity are still unclear. In earth gravity, buoyancy is an important parameter that affects boiling heat transfer through the rate at which bubbles are removed from the surface. A simple model describing the bubble departure size based on a quasi-static force balance between buoyancy and surface tension is given by the Fritz [1] relation:

$$Bo^{1/2} = 0.0208\theta$$

where Bo is the ratio between buoyancy and surface tension forces. For small, rapidly growing bubbles, inertia associated with the induced liquid motion can also cause bubble departure. In microgravity, the magnitude of effects related to natural convection and buoyancy are small and physical mechanisms normally masked by natural convection in earth gravity such as Marangoni convection can substantially influence the boiling and vapor bubble dynamics.

CHF is also substantially affected by microgravity. In 1-g environments, Bo has been used as a correlating parameter for CHF. Zuber's [2] CHF model for an infinite horizontal surface assumes that vapor columns formed by the merger of bubbles become unstable due to a Helmholtz instability blocking the supply of liquid to the surface. The jets are spaced λ_D apart, where

$$\lambda_D = 2\pi\sqrt{3}\left[\frac{\sigma}{g(\rho_l - \rho_v)}\right]^{1/2} = 2\pi\sqrt{3}LBo^{-1/2} = \sqrt{3}\lambda_c$$

and is the wavelength that amplifies most rapidly. The critical wavelength, λ_c, is the wavelength below which a vapor layer underneath a liquid layer is stable. For heaters with Bo smaller than about 3 (heaters smaller than λ_D), the above model is not applicable, and surface tension effects dominate. Bubble coalescence is thought to be the mechanism for CHF under these conditions. Small Bo can result by decreasing the size of a heater in

* Corresponding author. Tel.: +1-301-405-5437; fax: +1-301-314-9477.
E-mail address: kimjh@eng.umd.edu (J. Kim).

0017-9310/02/$ - see front matter © 2002 Published by Elsevier Science Ltd.
PII: S0017-9310(02)00108-4

Nomenclature

A	constant
a	acceleration
CHF	critical heat flux
Bo	Bond number $\left[=\frac{g(\rho_l-\rho_v)L^2}{\sigma}\right]$
f	frequency
g	acceleration of gravity
g_{osc}	amplitude of acceleration
L	length scale
q_{raw}	heat flux determined from the heater voltage, resistance, and area
q_{sc}	heat flux into the substrate
q_{rad}	radiant heat flux from the surface to the liquid
r	bubble radius
t	time
T_{bulk}	bulk liquid temperature
T_{sat}	saturation temperature
T_w	wall temperature
ΔT_{sat}	wall superheat
ΔT_{sub}	liquid subcooling
x	displacement

Greek symbols

λ_c	critical wavelength
λ_D	most dangerous wavelength
v	kinematic viscosity
θ	contact angle in degrees
ρ_l	density of liquid
ρ_v	density of vapor
σ	surface tension

earth gravity, or by operating a large heater in a lower gravity environment. In the microgravity of space, even large heaters can have low Bo, and models based on Helmholtz instability should not be applicable. The macrolayer model of Haramura and Katto [3] is dimensionally equivalent to Zuber's model and has the same dependence on gravity, so it should not be applicable as well. The goal of this work is to determine how boiling heat transfer mechanisms in a low-g environment are altered from those at higher gravity levels.

1.1. Literature review

Many of the early experimental studies regarding boiling heat transfer in microgravity environments were first performed under NASA sponsorship in drop towers (see [4,5] for a review), and were mainly concerned with determining the effect of gravity on the boiling process. The results of these early experiments were somewhat contradictory, with some experiments showing no effect of gravity on heat transfer and others showing a strong dependence. Much of the discrepancy can be attributed to the relatively short test times that were available since natural convection from before drop initiation could not be eliminated during the short drop time. Visual observations of the boiling process, however, revealed that a large increase in bubble size (up to a few millimeters) occurred under microgravity conditions, with small bubbles coalescing into larger bubbles a small distance from the heater. Siegel and Keshock [6], for example, found that the bubble departure radius varied approximately as $a^{-1/3}$ for $0.1 < a/g < 1$, and according to $a^{-1/2}$ for lower gravities.

Straub and co-workers have been looking at boiling in microgravity environments since the early 1980s [7–10]. Investigations were carried out using sounding rockets (test times of up to 6 min) under the TEXUS program, and using NASA's KC-135 aircraft (test times of about 25 s per parabolic flight path). Boiling curves from wires and flat plates at saturated and subcooled conditions were obtained for Freon 12, Freon 113, and water. Their results indicate that gravity has little effect on the overall heat transfer from flat plates, i.e., heater temperatures remained constant for given heat fluxes for $\pm 0.03 < a/g < 1.8$, although large increases in the bubble departure radius were observed. Bubble departure was thought to occur as a result of the inertia imparted to the surrounding liquid during bubble growth, which subsequently pulled the bubble away from the heated surface. The researchers concluded that buoyancy effects are replaced by surface tension effects (coalescence and evaporation–condensation) in microgravity, so the overall level of heat transfer remains about the same. It was concluded by these authors that evaporation was the primary heat transfer mechanism. Nucleate boiling on a small, 1.41 mm diameter hemispherical heater and a 0.02 mm diameter wire was studied by Steinbichler et al. [11] on a Spacelab Mission LMS and a Get Away Special using Freon 134a. The results suggest that stable, saturated boiling is possible on heaters small compared to the container, in contrast to the findings of Ohta et al. [12] who found that vapor accumulation near the heater prevented stable, steady-state boiling. They pointed out that, in contrast to other studies, the dynamics of the vapor generated by their small heater were not restricted by the test cell. They attributed the high heat transfer coefficients in microgravity saturated boiling to several factors. First, while the nucleation sites on the hemispherical heater and on the wire were concentrated on the top surface of the

heater in earth gravity, they were evenly distributed over the entire surface in microgravity. Bubble coalescence and turbulence in the fluid aid vapor removal from the surface. In low subcooled boiling, strong thermocapillary flows were observed to hold the bubbles onto the surface that supported the condensation/transport of vapor from the heated surface to the bulk fluid. During highly subcooled boiling, rapid growth and collapse of the bubbles on the surface were observed. Critical heat flux levels were observed to decrease with decreasing gravity, but the use of constant heat flux heaters precluded quantitative measurement of critical heat flux levels with accuracy.

Lee and Merte [13] describe the results of boiling experiments using R-113 from five space flights between 1992 and 1996. They used a gold film (19 mm × 38 mm) sputtered on a quartz substrate as both heater and temperature sensor. Boiling behavior under a wide range of heat fluxes and subcoolings were obtained. They observed eventual dryout of the surface under high heat fluxes at saturated conditions, but steady nucleate boiling at the same heat flux when the subcooling was increased to 22 °C. When steady nucleate boiling was observed, a very large bubble above the surface acted as a vapor sink for numerous smaller bubbles growing on the heater surface. The large bubble maintained its size due to a balance between condensation at the top of the bubble and coalescence with the smaller bubbles at its base. Enhancements in the heat transfer of up to 32% were observed in microgravity compared to earth gravity. Marangoni convection was also observed to play a significant role in the enhancement of heat transfer since it caused large vapor bubbles to be impelled toward the heater surface and small bubbles to migrate to the heater surface. Increased subcooling was associated with an increase in heat transfer level. CHF appeared to decrease significantly in microgravity.

Ohta et al. [14] measured the heat transfer, local temperature, and local liquid film thickness during boiling of ethanol on a sapphire substrate using a NASDA TR-1A rocket. The local heat transfer was calculated using a numerical simulation of the transient heat conduction within the central 50 mm of the sapphire substrate. The boundary condition information was provided by a row of platinum, thin film temperature sensors deposited directly onto the surface of the substrate. At saturated boiling, a very large bubble on the order of the test vessel size formed above the heater surface, and was "lifted" from the surface by numerous smaller "primary" bubbles. The authors did not observe a macrolayer. Boiling never reached a steady state since the primary bubbles grew and collapsed at regular intervals. The high heat transfer was attributed to the extending microlayer and dry spot as the primary bubbles grew without a corresponding increase in the dry spot. At high subcooled boiling, small bubbles on the heater surface were observed. Condensation occurred along the top of the bubbles, and steady state boiling was felt to occur.

Dhir et al. [15] documented the behavior of single sliding bubbles on downward facing surfaces at various inclinations. A single artificial cavity formed on a polished silicon wafer was used to generate the single bubble. Numerical simulations of the bubble growth and departure were performed at various gravity levels. They found that time and length scales in microgravity were stretched compared to earth gravity.

Di Marco and Grassi [16] investigated the effect of gravity on CHF during boiling on a wire using a parabolic aircraft. Wires of various sizes were tested under different gravity and pressure levels using both R113 and FC-72. They found that correlations in the literature gave acceptable predictions for high *Bo* at various length scales and gravity levels, but could not account for the data at low-*g* levels. They suggested that the CHF mechanism could change in low-*g* environments, and that additional terms containing gravity and wire diameter were needed to account for the different heat transfer mechanism.

Kim et al. [17] investigated saturated pool boiling of FC-72 using in a KC-135 using a 2.7 mm × 2.7 mm microheater array. Space- and time-resolved heat flux maps were obtained and correlated with video pictures of boiling on the surface recorded from below. Array averaged heat fluxes in low-*g* were slightly larger than in earth gravity for wall superheats up to about 30 K, but were significantly lower than in earth gravity at higher superheats. The time-average heat flux conditionally sampled on boiling, however, was independent of the gravity level suggesting that the behavior of small bubbles were not affected by gravity. Heat transfer from the surface occurred primarily through these small bubbles. Kim and Benton [18] studied highly subcooled boiling using a similar apparatus on a sounding rocket and a KC-135. The size of the primary bubble increased with increasing wall superheat. Most of the heaters under the primary bubble indicated low heat transfer due to local dryout on the heater surface. High heat transfer was associated with the three-phase contact line and the area surrounding the primary bubble where nucleate boiling occurred. Strong Marangoni convection around the bubble was observed to develop in low-*g*, forming a "jet" of fluid into the bulk liquid. The heat flux associated with the small bubbles was invariant with gravity.

1.2. Objectives

The experiments to date have shown that stable, subcooled boiling on flat plates in microgravity environments is possible, although usually with some alteration in heat transfer coefficients. It is important to note,

however, that almost all research pertaining to boiling in microgravity environments thus far has been of a qualitative nature (photographic studies) with some wall heat flux/wall temperature measurements, analytical work, or numerical simulations. In the studies where heat transfer coefficients were measured, the heated surfaces were always comparable to or larger than the individual bubbles, enabling only time and space averaged heat transfer and temperature to be obtained. Very little experimental data is available regarding the *local* heat transfer rates under and around the bubbles as they grow and depart from the surface. Better understanding of the heat transfer mechanisms involved in the boiling process can be attained by measuring when and where in the bubble departure cycle large amounts of heat are removed from the wall, and correlating this information to visual observations of the state of the bubble at those times. Another technologically important area in which little research has been performed is the effect of microgravity on critical heat flux. Although it is known that decreasing gravity decreases the critical heat flux level (e.g. [19]), relatively little quantitative data is available. Improved knowledge of the mechanisms controlling the boiling process will improve the reliability and performance of space based heat removal equipment.

The experiment described in this paper uses an array of microheaters to measure the local heat transfer on the surface during boiling. Each heater is on the order of the bubble departure size in normal gravity, but significantly smaller than the larger bubbles formed in reduced gravity. These heaters are individually controlled to operate at a constant temperature, allowing one to operate at CHF and into the transition boiling region without danger of heater burnout.

The objectives of the experiment were to determine the boiling heat transfer behavior in a low-g ($0.02g$) environment at various bulk fluid subcoolings, and to compare this behavior to those at $1g$ and high-g (1.6–$1.8g$) levels. Measurements were made from the nucleate boiling regime through CHF and into the transition boiling regime.

2. Experimental apparatus and procedure

2.1. Heater array

Local heat flux measurement and temperature control was performed using an array of platinum resistance heater elements deposited on a quartz wafer in a 2serpentine pattern. Each of these elements was $0.27\ \text{mm} \times 0.27\ \text{mm}$ in size, had a nominal resistance of $1000\ \Omega$, and a nominal temperature coefficient of resistance of $0.002\ ^\circ\text{C}^{-1}$. Ninety-six individual heaters were arranged in a square array about 2.7 mm on a side. The reader is referred to [20] for details.

2.2. Electronics

The temperature of each heater in the array was kept at a constant temperature by a bank of feedback circuits similar to those used in constant temperature hot-wire anemometry (see Fig. 1 for a schematic of one circuit). The electronics used in this series of tests were similar to those used in previous tests, and are described in [21], but were redesigned so that there were four feedback boards each containing 24 circuits and one data acquisition/control card. The op-amp measured the imbalance in the bridge and output whatever voltage was needed to keep the ratio R_h/R_u equal to the resistance ratio on the right side of the bridge.

The heater resistance, and thus the heater temperature, was controlled by varying the resistance of a digital potentiometer from Dallas Semiconductor (DS1267). This chip consists of two 10 kΩ digital potentiometers, each having 256 wiper positions. The two potentiometers were connected in series to make a single 20 kΩ potentiometer with 512 wiper positions. Control of the wiper position was performed through a three-wire serial interface to a personal computer and digital I/O card. For the resistor values indicated, a heater of nominally 1000 Ω resistance could be varied by ≈175 °C in ∼0.34 °C increments. The output of the circuit (V_{out}) was the time varying voltage across the heater.

The data acquisition system was a custom built unit that multiplexed the output signals of the individual feedback circuits, enabling the individual circuits to be sampled in any order. To acquire the output signal of a particular circuit, the address of that circuit was output from the computer to the data acquisition card, which then acquired a single sample from that circuit. The maximum sampling rate for the data acquisition was 50

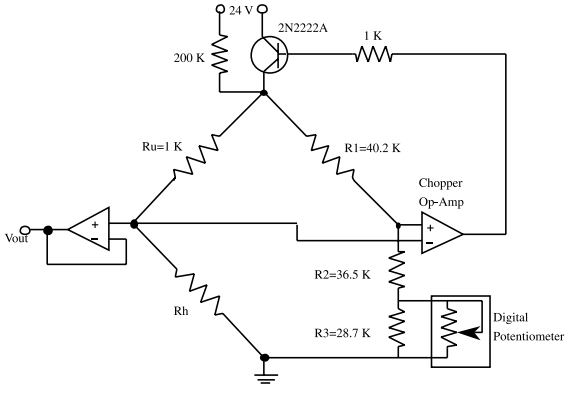

Fig. 1. Schematic of feedback loop.

kHz. Each heater could be sampled at a maximum rate of 500 Hz if all 96 circuits were being sampled.

2.3. Payload

Shown in Fig. 2 is a schematic of the boiling rig used in this study. This rig was originally developed for a sounding rocket payload that was flown in December 1999 [18]. It was subsequently modified so it could be flown on the KC-135. All the measurements described in this paper were obtained on the KC-135 during the first week of May 2001.

The bellows and the surrounding housing allowed the test section pressure to be controlled. A pump was used to break up stratification within the test chamber, while a PID temperature controller, a thermistor, and Kapton heaters attached to the boiling chamber were used to control the bulk fluid temperature. Although the fluid temperature lagged the sidewall temperature during heating by as much as 2 °C, the fluid and temperature and the sidewall temperature never differed by more than 0.1 °C once the bulk fluid temperature stabilized.

The test chamber was filled with nominally 3 l of distilled FC-72. The fluid was degassed by periodically pulling a vacuum on it over a two day period. The final dissolved gas concentration in the liquid, determined using the chamber temperature and pressure, the thermophysical properties of FC-72, and Henry's law, was $<1.5 \times 10^{-3}$ moles/mole. Gas concentrations smaller than 2×10^{-3} moles/mole have been shown to have no influence on the boiling behavior [22] in earth gravity. It has been argued that the presence of even minute amounts of dissolved gas can cause formation of Marangoni convection around vapor bubbles in subcooled environments [23]. Strong Marangoni convection was observed in the present data, as discussed below. Unfortunately, no information is currently available regarding the influence of Marangoni convection on boiling heat transfer in microgravity so we cannot determine the extent to which the data was influenced by the small amount of dissolved gas.

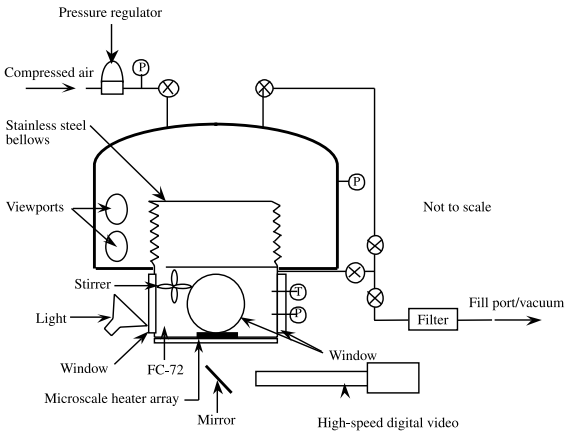

Fig. 2. Schematic of boiling rig.

The heater array was cooled from the bottom using an air jet at ambient temperature with a flow rate of 230 cc/s through a 1.6 mm diameter nozzle to prevent individual heaters from shutting off at low heat transfer levels (such as occurs when a large bubble covers the heater). The air jet offsets the heat transfer data for each heater in the array upward a fixed amount. This offset is measured and subtracted from the heat flux signal during data reduction to find the actual heat transfer from the heater surface to the liquid.

A high-speed digital video camera (Vision Research Phantom v4.1) imaging 250 frames per second at 512×512 pixels with a shutter speed of $1/1000$ s was used along with a long range microscope lens (Infinity KC with IF-3 objective) to obtain images of the boiling process through the bottom of the heater array. The camera buffer could store 2048 frames. Once the buffer was full, the stored images were played back to a hand-held mini-DV camcorder and recorded on tape. Another 30 Hz CCD camera and mini-DV camcorder were used to obtain pictures of the boiling process from the side. Control of the data acquisition was performed using a PC-104 based 233 MHz computer (Real Time Devices CMW686GX233-64). A 160 MB PCMCIA flash disk was used for data storage. Acceleration data in three directions were obtained using a three-axis accelerometer (Entran EGCS3) with a sensitivity of 2.5 V/g and a frequency response from 0 to 90 Hz. The accelerometer was mounted so that the z-axis was normal to the floor of the aircraft, the x-axis was fore to aft, and the y-axis port to starboard. Acceleration data was obtained at 50 Hz throughout the data acquisition time.

An external trigger was used to trigger the high-speed camera. This trigger signal was recorded along with the heat transfer and acceleration data, allowing the high-speed video to be synchronized with the data. Synchronization of the side-view video with the data was performed by flashing the LEDs used to light the boiling chamber (a 4 bit combination of short and long flashes) to indicate the run number followed by continuous illumination during data acquisition.

2.4. Test procedure

A typical parabolic maneuver on the KC-135 consisted of a high-g pull up for 25 s, a low-g period of 25 s, followed by a high-g pull out for 25 s. About 40 parabolas were performed on a given flight. The pump was turned off about 10 s before the start of a data run so fluid motion within the chamber could damp out. Data acquisition for a particular wall temperature was initiated during the transition from high-g to low-g using the

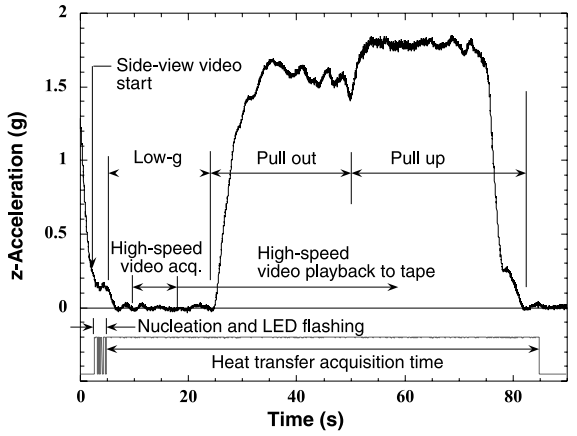

Fig. 3. Sequence of events during a typical data run.

same trigger signal used to acquire acceleration data. This was followed shortly by the start of recording of the side-view video. The heat transfer data acquisition program was initiated near the start of the low-g period. The wall temperature was set to a high value (typically 115 °C) for 2 s to initiate boiling on the surface followed by a drop in heater temperature to the desired wall temperature. The LEDs in the boiling chamber were flashed to indicate the run number, which typically took about 2 s. Data from the heaters in the array were then obtained for 80 s for the remainder of the low-g period, through the high-g pullout and pull up, and into the following low-g period. High-speed videos were obtained about 5 s after the heat transfer data acquisition started. Playback of the high-speed video onto tape occurred as soon as the camera buffer was full. A typical data run lasted 90 s. Once data acquisition was complete, the pump was turned on again. A representative acceleration profile in the z-direction throughout a data run indicating the sequence of events is shown in Fig. 3.

3. Data reduction and uncertainty analysis

The power supplied to the heater can be calculated from the voltage across the heater and the heater resistance (q_{raw}). Part of this power is lost through the substrate by conduction (q_{sc}), and part is transferred to the fluid (q). Since the latter quantity is what is desired, q_{raw} must be corrected to account for substrate conduction. The magnitude of this correction was determined as explained below.

The processes associated with boiling on any given heater can be identified from the heat flux variation with time. The term "boiling" in this work refers to the rapid growth and removal of bubbles, either by coalescence or buoyancy (in earth gravity), as indicated by the heat flux traces. The term "liquid" refers to liquid coming into contact with a heater without phase change for a relatively long time—such a situation could occur under natural convection conditions, or on a heater that is not influenced by bubbles nucleating around it. The term "vapor" refers to vapor coming into contact with the heater for a relatively long time—such a situation could occur when a large bubble covers a heater. The heat transfer from the wall to the fluid is very low in this case since the vapor insulates the surface.

Times when vapor covered the surface could be identified by the characteristically low and relatively steady heat flux—some examples are shown in Fig. 4. Heat flux traces and the corresponding video revealed that boiling on any individual heater was interrupted by periods of low heat flux during which vapor covered the heater. Heat transfer to the bulk liquid during this time was minimal since the heaters were effectively insulated from the liquid, and the measured heat transfer was taken to be the substrate conduction (q_{sc}). Because the heater temperature is held constant, q_{sc} is also constant independent of whether liquid contacts the heater, and could be subtracted from q_{raw} to obtain the heat flux from the wall to the fluid. The distribution of q_{sc} on the surface for a typical case is shown in Fig. 5. Higher values are observed towards the edge of the array and in the corners, as expected.

When the measured value of q_{sc} during the low-g period was subtracted from q_{raw} taken throughout the parabola to obtain q, q was observed to drop below zero periodically for a few (up to 5) heaters in the array during the high-g portion of the parabola. This is most likely due to cross-talk between the heaters in the array. When small non-uniformities in wall heat transfer occur, perhaps due to a bubble covering a portion of a heater, this can result in non-uniform temperatures across a heater and drive substrate conduction on the scale of an

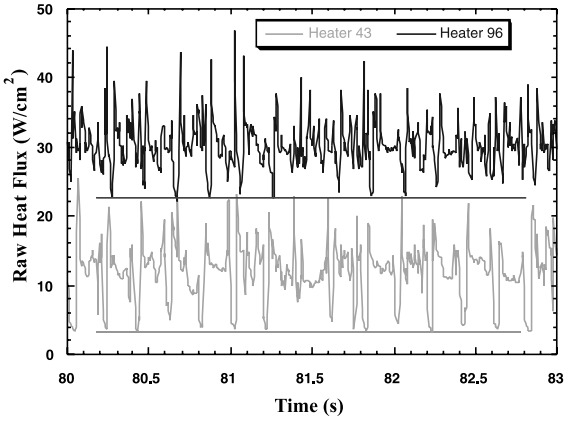

Fig. 4. Heat flux trace for two heaters in the array.

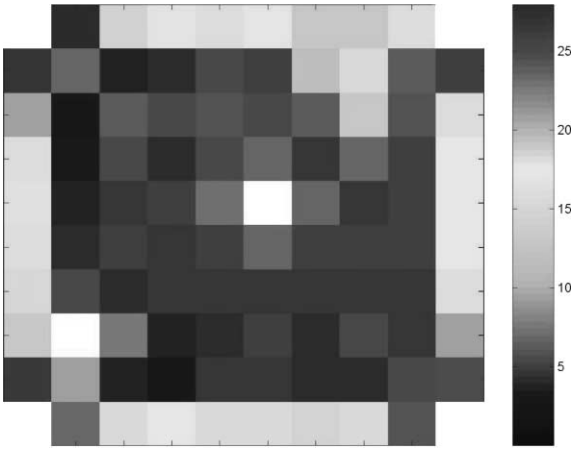

Fig. 5. Distribution of substrate conduction for $T_{bulk} = 30.9$ °C and $T_{wall} = 82.3$ °C. Non-functional heaters are colored white.

individual heater and cause an adjacent heater to dissipate heat at a rate different from what it would nominally be. The heat flux from any heater in the array never dropped more than 2 W/cm^2 below zero, however, which is much smaller than the heat flux magnitudes observed in the trace.

The uncertainty in q_{raw} is small since the voltage and heater resistance are known accurately. Higher uncertainties are associated with the partitioning of q_{raw} into q_{sc} and q. When vapor covers the heater, energy is lost by conduction into the vapor (q_{vap}) and by radiation (q_{rad}) between the wall and liquid. An upper limit for q_{vap} can be estimated assuming a vapor conductivity equal to that of the liquid, a vapor layer thickness of 0.5 mm, and a temperature difference between the maximum wall temperature (101.7 °C) and the saturation temperature of the liquid. This very conservative estimate yields $q_{vap} = 0.5$ W/cm^2. An upper limit on q_{rad}, estimated by assuming a black wall at the maximum temperature emitting to a black liquid at saturation temperature, was calculated to be 0.05 W/cm^2. Both q_{vap} and q_{rad} are much smaller than the uncertainty associated with heater cross-talk, and can be neglected. The uncertainty in the boiling curves is dominated by the uncertainty due to heater cross-talk and is taken to be 2 W/cm^2.

Boiling curves at various gravity levels and subcoolings ($\Delta T_{sub} = T_{sat} - T_{bulk}$) are presented in terms of wall heat flux vs. wall superheat ($\Delta T_{sat} = T_w - T_{sat}$). Because the pressure at the heater array changes during the parabola from high-g to low-g due to the changing weight of the fluid column above the heater array, changes in T_{sat} occur during a parabola. This causes time varying changes in wall superheat between the high-g and low-g data even though they were taken at the same heater temperature within minutes of each other. T_{sat} was calculated from a measurement of the time-resolved pressure at the heater array and the saturation curve data as given in the 3M catalog (3M [24]). Because the pressure transducer is below the heater array, corrections to the pressure due to the height of the fluid column between the transducer and the heater array were made.

Uncertainties in wall superheat and degree of subcooling occur due to uncertainties in heater calibration (about 2 digital potentiometer positions, or 0.68 °C), and uncertainties associated with measurement of bulk fluid temperatures and pressures. The thermistor used to measure the fluid temperature and the RTD used to control the chamber sidewall temperature were calibrated in a constant temperature water bath using a NIST traceable liquid-in-glass thermometer to within 0.2 °C. The uncertainty in both wall superheat and subcooling are conservatively estimated to be 1 °C.

4. Results

The bulk fluid was heated to the desired temperature before takeoff, and held at that temperature throughout the flight. Measurements were made with wall temperatures varying between 101.7 °C down to 63.1 °C in nominally 5 °C increments. The measurements were then repeated. The test conditions for each flight are summarized in Table 1.

4.1. Low-g environment

A typical acceleration profile throughout a test run was shown in Fig. 3. The rms accelerations during the low-g periods averaged over the week of flying were measured to be $g_{x,\mathrm{rms}} = 0.010g$, $g_{y,\mathrm{rms}} = 0.013g$, and $g_{z,\mathrm{rms}} = 0.026g$. FFTs of the acceleration in all three directions during a typical low-g period is shown in Fig. 6. Large peaks in the spectrum are observed between 0.1 and 0.3 Hz, consistent with the fluctuations seen in the z-acceleration in Fig. 3.

The effect of g-jitter on bubble motion can be estimated by calculating the magnitude of bubble oscillation when subjected to a sinusoidally varying g-field. Ishikawa et al. [25] studied the effect of bubble response to

Table 1
Summary of test conditions for each flight

Flight no.	T_{bulk} (°C)	Saturation temperature (°C) (subcooling level (°C))		
		Low-g	High-g	1-g
1	39.5	59.5 (20.0)	61.2 (21.7)	61.2 (21.7)
2	49.6	56.6 (7.0)	57.9 (8.3)	58.2 (8.6)
3	30.9	56.3 (25.4)	57.6 (26.7)	57.8 (26.9)
4	23.0	55.6 (32.6)	56.9 (33.9)	56.9 (33.9)

The saturation temperatures for each g-level were calculated based on the measured average liquid pressure at the heater and the thermophysical properties.

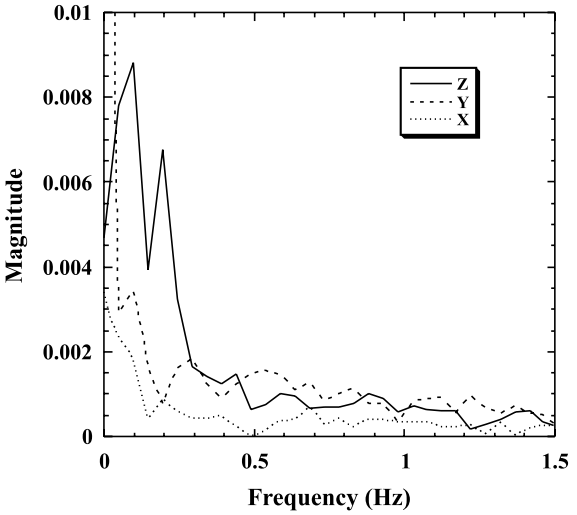

Fig. 6. Power spectrum of acceleration during a typical microgravity period.

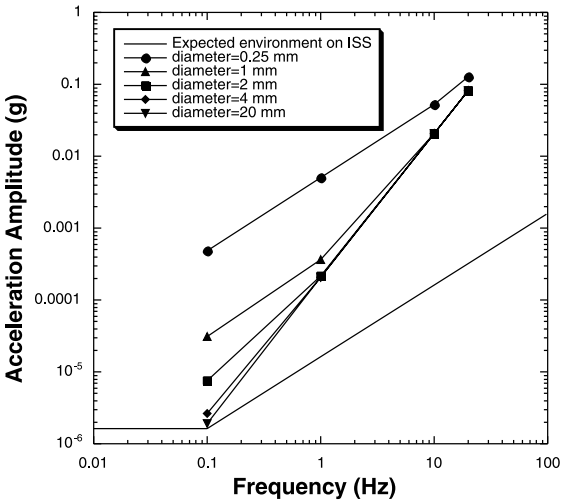

Fig. 7. Minimum acceptable acceleration vs. frequency for various bubble sizes. The expected environment on the ISS was obtained from Ref. [32].

periodic accelerations produced by a piezoelectric actuator within the microgravity environment produced by a TR-IA sounding rocket. Predicted displacements of the bubble agreed well with the measurements. The bubble position vs. time for a bubble subjected to a residual gravity of amplitude g_{osc} and frequency f was given by

$$x(t) = \frac{6\nu A}{2\pi f}\sin(2\pi f t) - r^2 A\left[\cos(2\pi f t) - \exp\left(\frac{6\nu}{r^2}t\right)\right]$$

where

$$A = \frac{2r^2 g_{osc}}{36\nu^2 + r^4(2\pi f)^2}$$

The bubble motion in the present test is complicated by the presence of a wall, but the above equation can be used to obtain an order of magnitude estimate of the bubble motion. Calculations were carried out for vapor bubbles 0.25–20 mm in diameter in FC-72. The acceleration level required to produce a displacement of 100 μm (about 40% of an individual heater size) in the bubble motion was determined for varying frequencies. A plot of the g-level vs. frequency is shown in Fig. 7. Bubbles attached to a wall will not move as much as indicated by Fig. 7 since surface tension retards bubble motion. Smaller bubbles are less susceptible to the effects of g-jitter, but even bubbles as small as a single heater can be affected by the g-jitter on the KC-135. The expected g-jitter environment on the ISS is seen to be acceptable for boiling studies.

4.2. Visual observations

Single frames from the high-speed video over the entire range of test conditions obtained through the bottom of the heater are shown in Fig. 8. A large primary bubble is seen to form whose size is on the order of the heater array. This bubble formed from the coalescence of smaller bubbles that grew on the surface after transition into low-g. The primary bubble increases in size with increasing bulk fluid temperature and wall superheat, and is fed by smaller satellite bubbles that surround it. For a given bulk temperature, the size of the satellite bubbles decreases with increasing superheat since the size to which they are able to grow is limited by the increasing size of the primary bubble. The satellite bubbles themselves were surrounded by even smaller bubbles which fed them, resulting in an almost fractal pattern to the boiling process. This suggests an approach to modeling low Bo boiling (boiling in low-g or on small heaters in earth gravity) where a large primary bubble forms that is fed by smaller bubbles, which in turn are fed by even smaller bubbles. Larger heaters would simply have a primary bubble with a larger length scale. The formation of a primary bubble similar in size to the heater surrounded by satellite bubbles of a range of sizes were also observed in videos of microgravity boiling taken by Merte and Chiaramonte [26] on a rectangular heater 19.1 mm × 38.1 mm.

The motion of the primary bubble at low bulk temperatures was less influenced by g-jitter since it was smaller and moved about the surface due to coalescence with the satellite bubbles. The size of the primary bubble is determined by a balance between vapor addition by evaporation of liquid at the bubble base and coalescence with satellite bubbles, and vapor removal by condensation through the bubble cap.

Side-view images at selected conditions are shown in Fig. 9. Marangoni convection around the bubble was

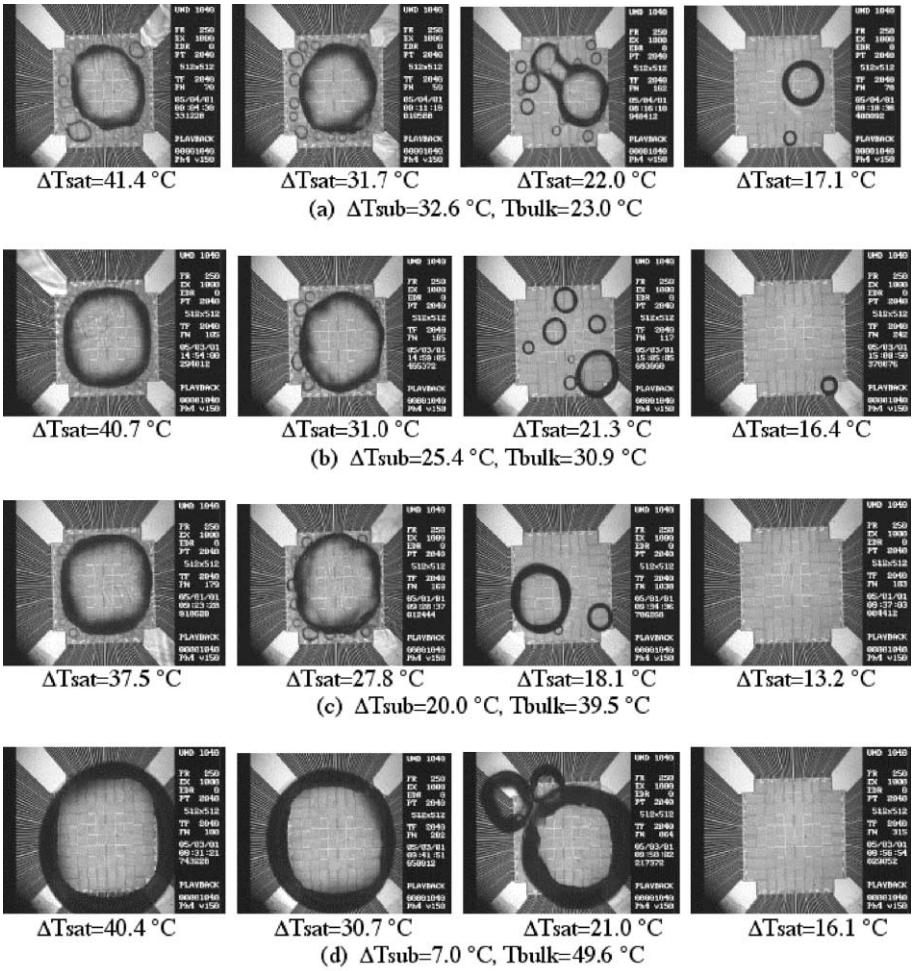

Fig. 8. Pictures of the bubble from below.

observed to develop, forming a "jet" of liquid into the bulk liquid. This jet also provided a reaction force on the primary bubble, keeping it on the heater. The strength of the Marangoni convection increased with increasing subcooling and wall superheat. Marangoni convection around vapor bubbles in subcooled boiling was also observed by Straub et al. [27] and Merte et al. [28].

Partial dryout under the primary bubble occurred for $\Delta T_{sub} = 20.0$ °C and higher. Dryout for the edge heaters did not occur, probably due to the flow induced by the Marangoni convection. Dryout over the entire heater array occurred for $\Delta T_{sub} = 7.0$ °C at $\Delta T_{sat} > 30.7$ °C. Dryout might have occurred as low as $\Delta T_{sat} = 25.7$ °C, but g-jitter caused the primary bubble to move slightly off the heater array, enabling liquid to rewet the edges of the heater. The contact line of the bubble was stable, and touched the outside of the heater array.

Bubble coalescence seems to be the mechanism by which CHF occurred under the conditions studied. No evidence of Taylor instability was observed at any of the test conditions. This is not surprising since the heater array size is much smaller than λ_D ($\sim$8 mm at 1g and $\sim$57 mm at 0.02g).

4.3. Boiling curves

Boiling curves for low-g, earth gravity, and high-g for various subcoolings are shown in Fig. 10. The high-g boiling curve is based on the middle 20 s of the high-g data, and includes data from the pull out ($\sim$1.6g) and pull up ($\sim$1.8g). Separate boiling curves were generated from the data taken during the pull out and pull up, but little difference in the curves was observed. The low-g curves are an average of all the data obtained during the first and second low-g periods.

The effect of g-jitter must be considered for the low-g curves. Higher wall superheat is generally associated with larger primary bubbles, which are more sensitive

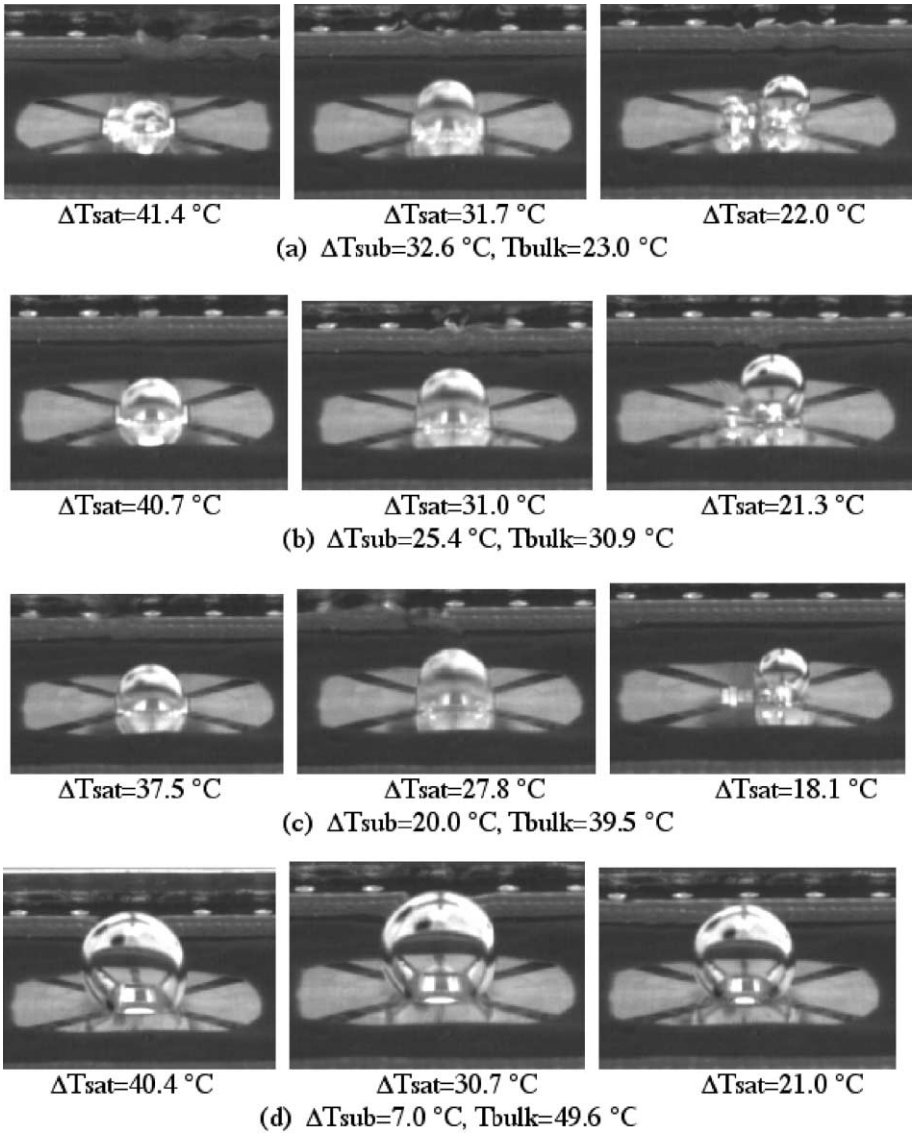

Fig. 9. Pictures of bubbles from the side.

to *g*-jitter. When the primary bubble moves on the surface or departs due to *g*-jitter, liquid rewets the surface and results in higher wall heat transfer than would occur in a true microgravity environment. The data at low subcooling and high wall superheats (especially those beyond CHF) may be artificially high as a result.

Little effect of subcooling is seen in the nucleate boiling regime for the 1*g* and high-*g* data, which is consistent with the observations of previous researchers. The low-*g* data tend to follow the 1*g* and high-*g* data for $\Delta T_{sat} < 20$ °C, but drop below them for higher superheats as the primary bubble causes dryout over a successively larger fraction of the heater. CHF for the low-*g* curves are significantly lower than those for the 1*g* and high-*g* data.

A plot of CHF vs. gravity and bulk fluid temperature is shown in Fig. 11. CHF is observed to increase with gravity and subcooling. The percentage increase in CHF over the $T_{bulk} = 49$ °C case, however, increases as the bulk temperature and gravity level decrease. Increased subcooling is seen to increase CHF dramatically, and there seems to be an increase in the wall temperature at which CHF occurs. Heater size effects on CHF under these conditions is not known. Experiments to address this are planned in the future.

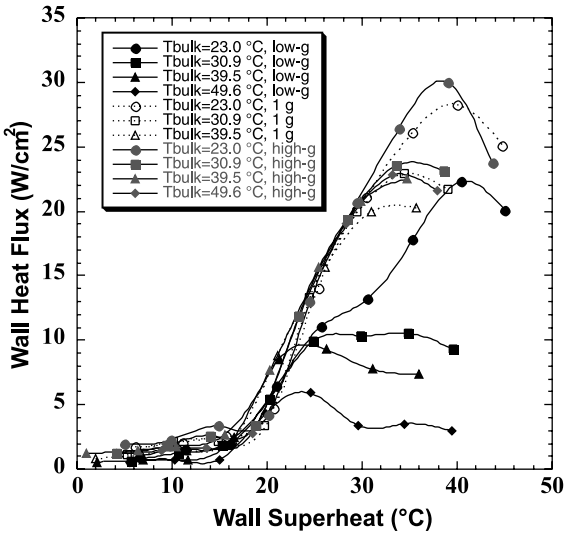

Fig. 10. Boiling curves at three gravity levels.

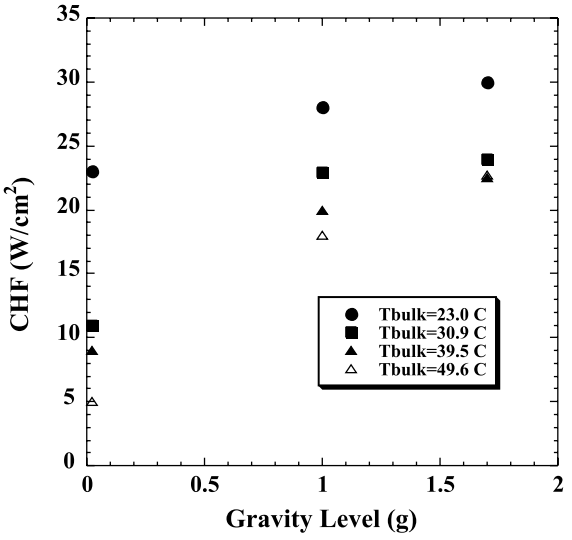

Fig. 11. Variation in CHF with gravity and subcooling.

Kutateladze [29] postulated that CHF in subcooled boiling should be increased above that required for saturated conditions by the amount of energy required to bring the subcooled liquid up to saturated conditions. He proposed a correlation of the form:

$$\frac{q_{\mathrm{CHF,sub}}}{q_{\mathrm{CHF,sat}}} = 1 + C_0\left(\frac{\rho_{\mathrm{l}}}{\rho_{\mathrm{v}}}\right)^{m}\frac{c_{\mathrm{pl}}(T_{\mathrm{sat}} - T_{\mathrm{l}})}{h_{\mathrm{fg}}}$$

Ivey and Morris [30] suggested $C_0 = 0.1$ and $m = 0.75$ based on available data. The above correlation indicates that gravity does not affect the enhancement in CHF. Using this correlation to normalize the CHF data in Fig. 11 to those at $\Delta T_{\mathrm{sub}} = 7.0$ °C according to

$$\frac{q_{\mathrm{CHF,sub1}}}{q_{\mathrm{CHF,sub2}}} = \left(\frac{q_{\mathrm{CHF,sub1}}}{q_{\mathrm{CHF,sat}}}\right)\Big/\left(\frac{q_{\mathrm{CHF,sub2}}}{q_{\mathrm{CHF,sat}}}\right)$$

results in the data shown in Fig. 12. A clear dependence on gravity is evident, indicating that the above correlation cannot be used to "correct" the effect of subcooling across gravity levels. An additional term that includes gravity needs to be included. A similar conclusion was made by Di Marco and Grassi [16] based on their study of boiling on wires in low-g.

4.4. Space resolved time-averaged heat flux

The time-averaged heat flux distribution across the array for the low-g data is shown in Fig. 13. The scale has been kept the same for all images to highlight the change in heat transfer with wall superheat and subcooling. Very little heat transfer is associated with the primary bubble. Much higher heat transfer rates are associated with the rapid growth and coalescence process of the satellite bubbles. A significant amount of the surface dries out before CHF. CHF occurs when the dry spot size grows faster than the increase in heat transfer outside the primary bubble. The time-averaged heat flux distribution at $\Delta T_{\mathrm{sub}} = 33.9$ °C and $\Delta T_{\mathrm{sat}} = 30.4$ °C for 1g is shown in Fig. 14 for comparison. Much more uniform heat transfer across the array is observed since the primary bubble is much less defined under these conditions. A significant reduction in the dry area is observed with increasing subcooling at a given superheat due to the increased amount of condensation through the primary bubble cap. The smaller primary bubble with increasing subcooling is directly related to the increase in CHF.

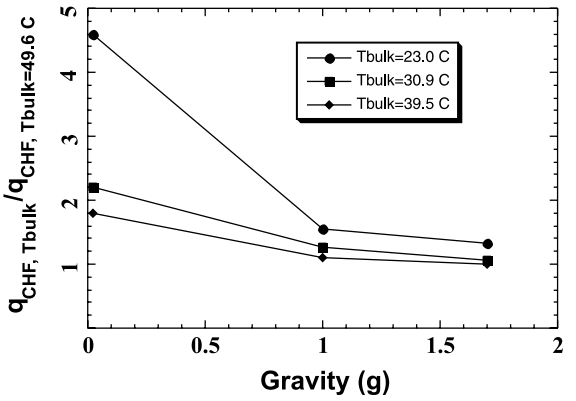

Fig. 12. Enhancement in CHF normalized on CHF at $\Delta T_{\mathrm{sub}} = 7.0$ °C.

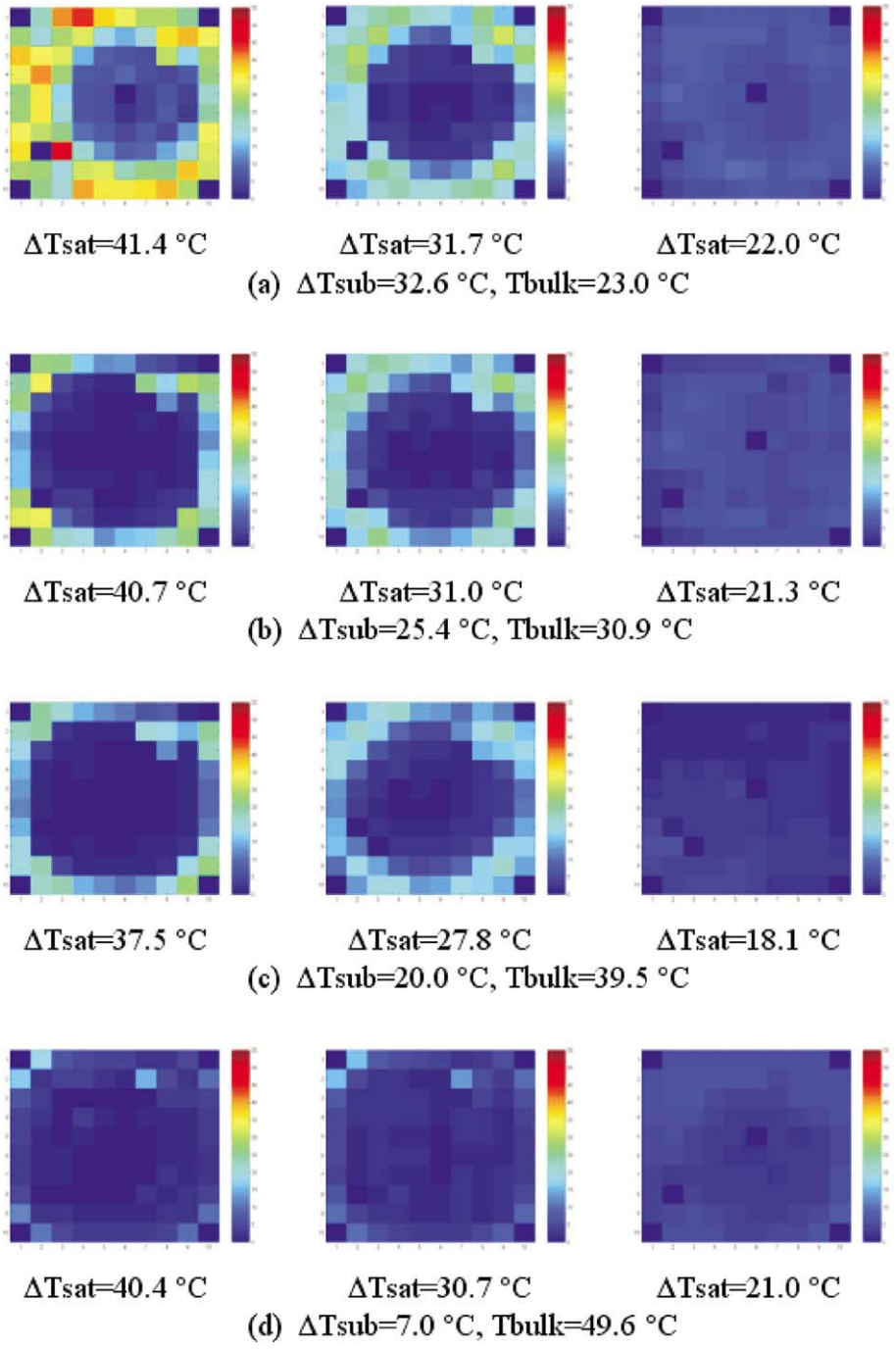

Fig. 13. Time average heat transfer distribution during low-g. The color scale varies between 0 and 55 W/cm^2.

4.5. Nucleate boiling heat flux

In order to conditionally sample the heat flux only when boiling occurs on the surface, a *boiling function* was generated from the time-resolved heat flux data. This function is a bimodal signal that is set to HIGH when boiling occurs on the surface, and LOW otherwise. Details of how the boiling function is generated are discussed in [20,31]. The time-average heat flux obtained by sampling the data only when the boiling function is

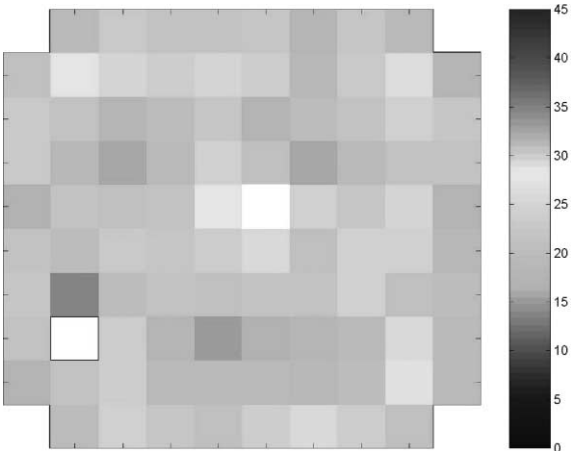

Fig. 14. Time average heat flux distribution at $\Delta T_{sub} = 33.9$ °C ($T_{bulk} = 23$ °C), and $\Delta T_{sat} = 30.4$ °C in 1*g*.

HIGH is referred to as the nucleate boiling heat flux, and is a measure of the heat transfer associated with the satellite bubbles.

One additional step was performed in processing the current results. Because a heater can be partially covered with vapor if the contact line of the primary bubble intersects it, the heat transfer signal may be declared HIGH if the thresholds are set low enough. The heat transfer in this case would be lower than on a heater that was fully wetted with liquid. To minimize the chance that the data from partially wetted heaters is included in the nucleation heat flux, software was written to determine the extent of the dry spot underneath the primary bubble at a given time—only data from those heaters that were at least one heater away in the radial direction from the dry spot were used in the calculation. Also, cases where significant nucleate boiling occurred on fewer than 10 heaters (e.g., $T_{bulk} = 49.6$ °C and $T_{sat} = 30.7$ °C where complete dryout occurred over the array) were discarded since a statistically representative sample was not available.

Boiling curves generated from the nucleate boiling heat flux for low-*g* and high-*g* environments are compared in Fig. 15. It is seen that the nucleate boiling heat flux collapse onto a single curve, indicating that the small scale boiling is independent of subcooling and gravity level. This suggests that if one is able to predict the extent of the dry area in low-*g*, then one can predict the low-*g* boiling curve from earth or high gravity boiling heat flux data.

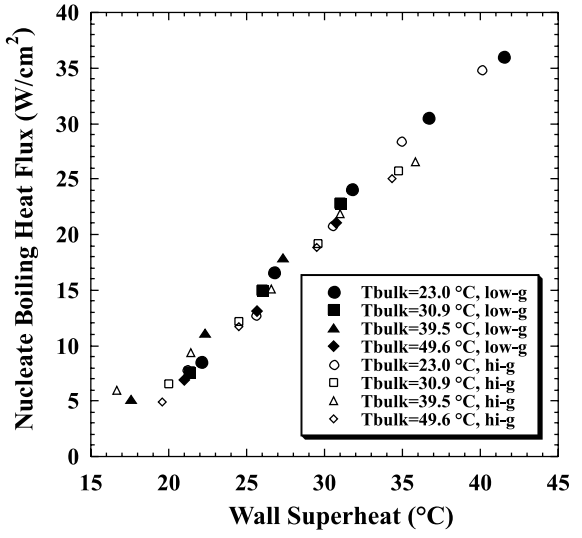

Fig. 15. Nucleate boiling heat flux.

5. Conclusions

Our observations to date indicate that low-*g* boiling heat transfer is dominated by the formation of a large primary bubble on the surface by the coalescence of smaller bubbles. Dryout occurs under the primary bubble, causing CHF in low-*g* to be significantly lower than in earth gravity. The primary bubble also limits the size of the smaller satellite bubbles, causing significant bubble activity and higher heat transfer rates. Subcooling was observed to have a strong effect on the size of the primary bubble and on CHF. CHF was observed to increase with higher subcooling and gravity level. Heat transfer associated with small-scale boiling was observed to be independent of subcooling and gravity level.

Acknowledgements

This work was funded by NASA Headquarters under Grant NCC3-783. The grant monitor is Mr. John McQuillen.

References

[1] W. Fritz, Berechnungen des Maximalvolumens von Dampfblasen, Phys. Z. 36 (1935) 379–384.
[2] N. Zuber, Hydrodynamics of Boiling Heat Transfer, AEC Report AECU-4439, 1959.
[3] Y. Haramura, Y. Katto, A new hydrodynamic model of the critical heat flux, applicable widely to both pool and forced convective boiling on submerged bodies in saturated liquids, Int J. Heat Mass Transfer 26 (1983) 389–399.
[4] R. Siegel, Effects of reduced gravity on heat transfer, in: Advances in Heat Transfer, vol. 4, Academic Press, New York/London, 1967, pp. 143–228.
[5] J.A. Clark, Gravic and agravic effects in cryogenic heat transfer, Adv. Cryogen. Heat Transfer 87 (64) (1968) 93–102.

[6] R. Siegel, E.G. Keshock, Effects of reduced gravity on nucleate boiling bubble dynamics in saturated water, J. A.I.Ch.E. 4 4 (10) (1964) 509–517.
[7] M. Zell, J. Straub, A. Weinzierl, Nucleate pool boiling in subcooled liquid under microgravity results of texus experimental investigations, Proceedings of the 5th European Symposium on Material Sciences under Microgravity, Schloss Elmau, ESA SP-222, 1984, pp. 327–333.
[8] B. Vogel, J. Straub, Single bubble experiments in pool boiling, Proceedings of VIII European Symposium on Materials and Fluid Sciences in Microgravity, Brussels, Belgium, ESA SP-333, 1992, pp. 879–886.
[9] M. Zell, J. Straub, B. Vogel, Heat transfer in pool boiling under microgravity, Sov. J. Low Temp. Phys. 16 (5) (1990) 323–324.
[10] M. Zell, J. Straub, B. Vogel, Pool boiling under microgravity, J. Physicochem. Hydrodyn. 11 (5/6) (1989) 813–823.
[11] M. Steinbichler, S. Micko, J. Straub, Nucleate boiling heat transfer on a small hemispherical heater and a wire under microgravity, Proceedings of the 11th International Heat Transfer Conference, Kyongju, Korea, vol. 2, 1998, pp. 539–544.
[12] H. Ohta, M. Kawaji, H. Azuma, K. Kawasaki, H. Tamaoki, K. Ohta, T. Takada, S. Okada, S. Yoda, T. Nakamura, TR-1A rocket experiment on nucleate boiling heat transfer under microgravity, ASME-MEMS HTD 354 (1997) 249–256.
[13] H.S. Lee, H. Merte, Pool boiling phenomena in microgravity, Proceedings of the 11th International Heat Transfer Conference, Kyongju, Korea, vol. 2, 1998, pp. 395–400.
[14] H. Ohta, M. Kawaji, H. Azuma, K. Inoue, K. Kawasaki, S. Okada, S. Yoda, T. Nakamura, Heat transfer in nucleate pool boiling under microgravity condition, Proceedings of the 11th International Heat Transfer Conference, Kyongju, Korea, vol. 2, 1998, pp. 401–406.
[15] V.K. Dhir, D.M. Qui, N. Ramanujapu, M.M. Hasan, Investigation of nucleate boiling mechanisms under microgravity conditions, Proceedings of the Fourth Microgravity Fluid Physics and Transport Phenomena Conference, Cleveland, OH, 1998.
[16] P. Di Marco, W. Grassi, About the scaling of critical heat flux with gravity acceleration in pool boiling, XVII UIT National Heat Transfer Conference, Ferrara, June 30–July 2, 1999.
[17] J. Kim, N. Yaddanapuddi, J.D. Mullen, Transfer behavior on small horizontal heaters during saturated pool boiling of FC-72 in microgravity, Micrograv. Sci. Technol. 12 (2001) 116–127.
[18] J. Kim, J.F. Benton, Subcooled pool boiling heat transfer in earth gravity and microgravity, Int. J. Heat Fluid Flow 23 (4) (2002) 497–508.
[19] J. Straub, M. Zell, B. Vogel, Pool boiling in a reduced gravity field, Proceeding of the 9th International Heat Transfer Conference, Jerusalem, Israel, Hemisphere, 1990, pp. 91–112.
[20] T.D. Rule, J. Kim, Heat transfer behavior on small horizontal heaters during pool boiling of FC-72, J. Heat Transfer 121 (2) (1999) 386–393.
[21] S. Bae, M.H. Kim, J. Kim, Improved technique to measure time and space resolved heat transfer under single bubbles during saturated pool boiling of FC-72, Experiment. Heat Transfer 12 (3) (1999) 265–278.
[22] S.M. You, T.W. Simon, A. Bar-Cohen, Y.S. Hong, Effect of dissolved gas content on pool boiling of a highly wetting fluid, J. Heat Transfer 117 (1995) 687–692.
[23] J. Straub, Origin and effect of thermocapillary convection in subcooled boiling: observations and conclusions from experiments performed in microgravity, 2001 Engineering Foundation Conference on Microgravity Transport Processes in Fluid, Thermal, Biological and Materials Sciences II, Banff, CA, Paper MTP01-41.
[24] 3M Corporation, 3M Fluorinert Liquids Product and Contact Guide, 1995.
[25] M. Ishikawa, T. Nakamura, S. Yoda, H. Samejima, T. Goshozono, Responsive motion of bubbles to periodic *g*-jitter, Micrograv. Sci. Technol. VII (2) (1994) 164–168.
[26] H. Merte, F.P. Chiaramonte, Pool boiling experiment, NASA Glenn Research Center Video, GRC 396, 2001.
[27] J. Straub, G. Picker, J. Winter, M. Zell, Effective cooling of electrinic components by boiling phase transition in microgravity, Acta Astronautica 40 (2–8) (1997) 119–127.
[28] H. Merte, H.S. Lee, K.B. Keller, Dryout and Rewetting in the Pool Boiling Experiment Flown on STS-72 (PBE-II B) AND STS-77 (PBE-II A), NASA/CR, 1998, pp. 207–410.
[29] S.S. Kutateladze, Heat transfer during condensation and boiling, translated from a publication of the State Scientific and Technical Publishers of Literature and Machinery, Moscow-Leningrad, as AEC-TR-3770, 1952.
[30] H.J. Ivey, D.J. Morris, On the relevance of the vapor–liquid exchange mechanism for subcooled boiling heat transfer at high pressure, British Rep. AEEW-R-137, Atomic Energy Establishment, Winfrith, 1962.
[31] T.D. Rule, Design, construction, and qualification of a microscale heater array for use in boiling heat transfer, Master's Thesis, School of Mechanical and Materials Engineering, Washington State University, Pullman, WA, 1997.
[32] Specification Number SSP 41000E, System Specification for the International Space Station, prepared for NASA by the Boeing Defense and Space Group, 1996.